Atmos. Meas. Tech. Discuss., 5, 97–135, 2012
www.atmos-meas-tech-discuss.net/5/97/2012/
doi:10.5194/amtd-5-97-2012

Atmospheric Measurement Techniques Discussions

Particle sizing calibration with refractive index correction for light scattering optical particle counters and impacts upon PCASP and CDP data collected during the Fennec campaign

P. D. Rosenberg[1], A. R. Dean[2], P. I. Williams[3], A. Minikin[4], M. A. Pickering[5], and A. Petzold[4]

[1]School of Earth and Environment, University of Leeds, Leeds, LS2 9JT, UK
[2]Facility of Airborne Atmospheric Research, Cranfield, MK43 0AL, UK
[3]School of Earth, Atmospheric and Environmental Sciences, University of Manchester, Manchester, M13 9PL, UK
[4]Institute of Atmospheric Physics, DLR, 82234 Wessling, Germany
[5]Met Office, Exeter, EX1 3PB, UK

Received: 19 December 2011 – Accepted: 21 December 2011 – Published: 4 January 2012

Correspondence to: P. D. Rosenberg (p.d.rosenberg@leeds.ac.uk)

Published by Copernicus Publications on behalf of the European Geosciences Union.

AMTD
5, 97–135, 2012

Abstract

Optical particle counters (OPCs) are used regularly for atmospheric research, measuring particle scattering cross sections to generate particle size distribution histograms. This manuscript presents two methods for calibrating OPCs with case studies based on a Passive Cavity Aerosol Spectrometer Probe (PCASP) and a Cloud Droplet Probe (CDP), both of which are operated on the Facility for Airborne Atmospheric Measurements BAe-146 research aircraft.

A method is also provided for modification of OPC bin boundaries when the scattering properties of measured particles are different to those of the calibration particles due to differences in refractive index or shape. This method provides mean diameters and widths for OPC bins based upon Mie-Lorenz theory or any other particle scattering theory, without the need for smoothing, despite the highly nonlinear and non-monotonic relationship between particle size and scattering cross section. By calibrating an OPC in terms of its scattering cross section the optical properties correction can be applied with minimal information loss and full propagation of uncertainty.

Analysis of multiple calibrations has shown that for the PCASP the bin centres differ by up to 30 % from the manufacturer's nominal values and can change by approximately 20 % when routine maintenance is performed. The CDP has been found to differ from the manufacturer's specification by 15–64 % and over the course of the Fennec project in the Sahara the variability of calibration was always less than the 2-σ calibration uncertainty or 10 %.

As would be expected from Mie-Lorenz theory the impact of the refractive index corrections has been found to be largest for absorbing materials and the impact on Saharan dust measurements made as part of the Fennec project has been found to be up to a factor of 3 for the largest particles which could be measured by CDP.

Software tools have been developed as part of this work and are now made available as open source resources for the community via the SourceForge repository.

AMTD
5, 97–135, 2012

1 Introduction

1.1 Optical particle counters

Light scattering optical particle counters (OPCs) are instruments used to measure the concentration and size of airborne particles. They are used in many fields such as in ground based, aircraft based or balloon based atmospheric research or pollution or clean room monitoring. OPCs function by passing an air sample though a beam of light and detecting the radiation scattered out of the beam by individual suspended particles. OPCs have applications over a wide range of particle sizes from aerosol particles with diameters of 0.06 µm (Cai et al., 2008) to ice and liquid cloud particles with diameters of the order one-hundred micrometres (Cotton et al., 2010) although an individual instrument will usually cover a size range of approximately one to two orders of magnitude. Shadow OPCs provide size distributions up to mm sizes but are not discussed further here. Because of their ability to provide real-time data over many sizes ranges OPCs are the de-facto standard for measuring particle size distributions, particularly on research aircraft where their fast acquisition speeds are important.

Despite these advantages OPCs do not provide particle diameters explicitly. The amount of light scattered by a particle is defined not only by a particle's size but also by its shape, refractive index, n, (which may be complex in the case of light absorbing materials) and whether or not the particle is homogeneous. These additional variables are particularly important in atmospheric measurements where OPCs are often employed to measure many different particle types from spherical homogeneous water droplets ($n = 1.33$) to angular volcanic ash particles (n in the range $1.5–1.6 + 0.001\,i - 0.02\,i$ (Muñoz et al., 2004; Patterson, 1981; Patterson et al., 1983).

Designs of OPCs vary enormously; however there are some features which are common to almost all instruments. Each collects the scattered light over an angular range defined by the geometry of the instrument's optics and focuses this light onto a photo-detecting element. Each particle passing through the beam therefore generates an electrical pulse in a detector circuit. All OPCs measure the height of this pulse and

AMTD
5, 97–135, 2012

some measure other properties such as pulse width or shape. Some OPCs collate particle events into discrete time and/or pulse height bins while others provide the time and pulse height for every particle at the finest resolution allowed by the electronics.

Assuming an appropriate calibration is performed, the height of each pulse is a direct measurement of a particle's scattering cross section over the collecting solid angle of the OPC optics. Combining these measurements of particles' cross sections with knowledge of how cross section varies with size allows a size distribution to be derived. Performing an effective calibration and scattering properties correction is essential to generate the highest quality data from an OPC. The later of these is made more difficult because scattering cross section is often not a monotonic function diameter over much or the size range where OPCs are applied. This manuscript describes methods for calibrating OPCs and performing scattering properties corrections as well as providing software for performing these operations with examples taken from the instrumentation operated by the Facility for Airborne Atmospheric Measurements.

1.2 The passive cavity aerosol spectrometer probe and cloud droplet probe

The Facility for Airborne Atmospheric Measurements (FAAM) operates a number of OPCs on the UK's BAe-146-301 Atmospheric Research Aircraft. Amongst these are a Passive Cavity Aerosol Spectrometer Probe 100-X (PCASP) and a Cloud Droplet Probe (CDP) which are both mounted externally on the aircraft below the wings.

The PCASP was initially manufactured by Particle Measurement Systems but it has since been modified to include the SPP-200 electronics package manufactured by Droplet Measurement Technologies (DMT). Its manufacturer specification indicates it covers the range 0.1 to 3 µm diameter. It is a closed cell instrument meaning that it draws an air sample containing aerosol particles into an optical chamber where it makes its measurements.

The PCASP employs a He-Ne laser with wavelength 0.6328 µm as its radiation source and the sample is sheathed in clean air as it enters the optical chamber. The sheath focuses and constrains the particles to the centre of the laser beam and also

AMTD
5, 97–135, 2012

accelerates the sample, spreading particles in the direction of the flow and reducing particle coincidence effects. The laser is directed through the optical chamber across the sample and is incident upon a crystal oscillator where 0.1 % of the incident radiation passes through to a photodetector allowing measurement of the laser intensity and the remaining 99.9 % is reflected back along the reciprocal path. The use of an oscillator rather than a mirror ensures the direct and reflected beams are not coherent and ensures interference between the beams does not occur. The scattered light is collected by a parabolic mirror which collects light from the direct beam over the angular range 35–120° and from the reflected beam over the range 60–145° before a lens focuses it onto a photodetector. The signal from the photodetector is processed by three parallel systems; a high, mid and low gain stage, and the pulse height from each of these three stages is digitised to give a value of 1–4096 for the high gain stage, 4097–8192 for the mid gain stage and 8193–12 288 for the low gain stage. In the manufacturer specifications the three gain stages correspond to particle diameters of 0.1–0.14, 0.14–0.3 and 0.3–3.0 µm. Based on whether the particle registers or saturates on the different gain stages one single value is chosen to represent the pulse height in the range 1–12 288. Based on this pulse height the particle is assigned to one of 30 channels generating a histogram every 0.1, 1 or 10 s.

When operated on an aircraft the PCASP is fitted with a forward facing conical inlet. Air is forced into the nosecone by ram pressure and as the nosecone cross sectional area increases the mean air velocity decreases by a factor of ten. A small subsample of this air is drawn through a needle inlet for measurement and the remaining air passes through an overflow outlet to the side. The intention is that after deceleration the subsampler operates approximately isokinetically; however, this is affected by factors such as aircraft speed and altitude. To bring the sampling as close as possible to isokinetic over the range of altitudes flown by the FAAM BAe-146 the PCASP's sample flow rate at ground level has been increased to 3 $cm^3 s^{-1}$ from the manufacturer recommended setting of 1 $cm^3 s^{-1}$. This maintains the subsampling within the range covered by Belyaev and Levin (1974). The impact upon particle sizing and spreading

AMTD
5, 97–135, 2012

of the measured size distribution due to the increased flow rate have been assessed and found to be negligible. Despite matching the subsampler air velocity to the conical inlet mean air velocity, it is clear that the Reynolds number at the inlet tip may be as high as ~60 000 during flight which is an indicator that turbulence should be present. A 3-dimensional incompressible fluid dynamics model with direct numerical simulation of turbulence has confirmed that flow separation occurs in the conical inlet leading to turbulent eddies at the subsampler. Further investigation in terms of compressible fluid modelling, inlet comparison and wind tunnel testing will be required to assess the impact of this turbulence on the sampled size distribution.

The CDP is manufactured by DMT and is specified to detect and size cloud droplets with diameters from 3–50 µm. In contrast to the PCASP, which has an internal sampling system, the CDP is an open path OPC. It consists of two arms, separated by 111.1 mm, which house the detecting components of the system. A 658 nm diode laser is directed out of a sapphire window and between the two arms across an open sample area. In the sample area, particles suspended in an air sample pass through the beam and scatter laser radiation. The unscattered radiation and a subset of scattered radiation pass through a second sapphire window into the detector arm and the intensity of the unscattered beam is measured by a dump spot monitor. Light scattered within the range 4–12° is passed onto an optical beam splitter where 33 % and 67 % of the light is directed to two detectors known as the Sizer and Qualifier respectively.

To avoid the need for complex retrieval algorithms the CDP attempts to screen out all particles which do not pass through a small area of ~0.24 mm^2 located equidistant from the two arms and known as the instrument's depth-of-field. This is performed by placing a linear mask over the Qualifier detector meaning that the ratio of the Sizer to Qualifier signal is a function of particle position. For accepted particles the analogue Sizer signal is amplified and digitised and the pulse height is measured giving a value in the range 1–4096. For the first the first 256 particles recorded per second the particle incidence time and size at maximum resolution is recorded. Subsequent particles are added to a 1 Hz histogram with thirty bins based on pulse height.

AMTD
5, 97–135, 2012

Although the CDP is designed for use with water droplets it has been used to measure large aerosol, ash and dust particles. The impact of different compositions or shapes on the Sizer/Qualifier signal ratio has not been evaluated.

2 Calibration techniques

2.1 Sample generation and scattering cross section calculation

Because OPCs measure particle scattering cross section directly calibrations can be performed more easily in terms of this parameter. It is therefore critically important that the calibration particles have well defined scattering cross sections. The two most common types of calibration particles used are polystyrene latex (PSL) spheres and glass beads, both of which are commercially available in samples with very narrow distributions and may be suspended in air to provide a calibration sample. Those used here were calibrated using photon correlation spectroscopy and optical microscopy, traceable via NIST to the Standard Metre. Although these particles have the advantage of a traceable calibration certificate, they are only available in a finite number of discrete sizes. This is a particular problem for the PCASP high gain stage which does not span many available sizes of PSL spheres.

Aerosol particles with a broad distribution can also be used for calibration if a well defined subsample can be taken. Here this has been performed by passing the aerosol through a Differential Mobility Analyser (DMA). DMAs were first described by Knutson and Whiteby (1975). In brief, a DMA consists of a column with an inner and an outer cylindrical electrode with centres coaxially located. The outer electrode is grounded and separated from the inner electrode by a known distance and the column has two inlets and two outlets. The polydisperse sample inlet with flow rate Q_a is located at the column outer wall and the sheath inlet with larger flow rate Q_{sh} over the remaining column cross section. At the opposite end of the column the monodisperse sample outlet is located at the column centre and has an outward flow of Q_s and the excess flow

AMTD
5, 97–135, 2012

outlet covers the remaining column cross section with flow rate Q_s. A broad distribution of charged aerosol is introduced to the column via the polydisperse sample inlet and an electric field applied across the electrodes causes these particles to be deflected towards the column centre based on their electrical mobility, Z. Electrical mobility is defined by the stokes equation as

$$Z = \frac{n_e e\, C}{3\,\pi\,\eta D_p} \tag{1}$$

where e is the charge on an electron, n_e is the number of additional electrons on the particle, C is the Cunningham slip correction factor η is the dynamic viscosity of the carrier gas and D_p is the particle diameter. For a given column geometry, set of flow rates, and electric field only particles with a specific mobility will be deflected by the correct amount to pass through a narrow gap and out via the monodisperse outlet. By varying the flow rates or the electric field, particles of a particular mobility can be selected.

A DMA has a well defined, tuneable, transfer function which yields a narrow particle distribution that can be used for calibration. Under the most common configuration, as used in this work ($Q_{sh} = Q_e$ and $Q_a = Q_s$), the transfer function of a DMA as a function of electrical mobility has a triangular shape which can be described as

$$T \propto \max\left(0,\, 1 - \frac{|Z^* - Z|}{\Delta Z}\right), \tag{2}$$

where Z^* is the mid-point mobility of the distribution and ΔZ is the full width at half maximum of the transmission function. When operating a DMA the ΔZ is proportional to Q_a/Q_{sh} and Z^* is proportional to V/Q_{sh} where V is the electrode potential difference. This means, that for a fixed value of Q_a and a maximum achievable electric field, there is a trade-off between maximising the available aerosol sizes and maintaining a narrow distribution. For use with FAAM's PCASPs which draw at 3 $cm^3\,s^{-1}$ values of $\Delta Z/Z^*$ of around 5 % are achievable for particle diameters less than 0.5 µm.

AMTD
5, 97–135, 2012

A number of aerosol types have been used in this manner. The preferred aerosol is nebulised di(2-ethyhexyl)sebacate (DEHS) with a distribution much wider than the DMA transfer function. This material has a well known refractive index and forms stable spherical liquid aerosol particles, making it ideal for use with Mie-Lorenz theory calculations. One disadvantage is that DEHS is a plasticiser so can attack plastic components. Oleic acid and ammonium sulphate have been tested, but the former reacts with oxygen and the latter does not form perfectly spherical aerosol (Dick et al., 1998; Hudson et al., 2007).

Mie-Lorenz theory is used to derive the scattering properties of calibration particles as a function of their diameter and refractive index. Mie-Lorenz theory exactly describes the scattering of radiation by homogeneous spheres and here the scattering phase function is derived using the code of Wiscombe (1980). In general for a particle with diameter, D_p, and refractive index, n, the scattering cross section measured by an OPC is given by the integral of the phase function as

$$\sigma = \frac{\pi}{k^2} \int_0^{2\pi} \int_0^{\pi} \left(\left| S_1(\theta, k D_p, n) \right|^2 + \left| S_2(\theta, k D_p, n) \right|^2 \right) \sin(\theta)\, w(\theta, \phi)\, d\theta\, d\phi \quad (3)$$

where k is the wavenumber of the light used by the OPC, D_p is the particle's diameter, n is the particle's refractive index, $(\left|S_1(\theta, k D_p, n)\right|^2 + \left|S_2(\theta, k D_p, n)\right|^2)$ is the scattering intensity derived from Mie-Lorenz theory (split into light polarised parallel, S_1, and perpendicular, S_2, to the scattering plane), θ is the angle between the incident laser beam and the scattering direction, φ is the direction of the scattered radiation around the incident beam and $w(\theta, \varphi)$ is a weighting function defined by the optical geometry of the OPC. The value of $w(\theta, \varphi)$ varied from 0 at angles where no light is collected to 1 where all light is collected. In the PCASP where the beam is incoherently reflected back on itself $w(\theta, \varphi)$ may be greater than 1 and in the case of rotational symmetry around the laser beam w is a function of θ only. For the PCASP $w(\theta) = 1$ for $35^\circ < \theta < 60^\circ$ and $120^\circ < \theta < 145^\circ$, $w(\theta) = 2$ for $60^\circ < \theta < 120^\circ$ and $w(\theta) = 0$ otherwise. For the CDP $w(\theta) = 1$ for $4^\circ < \theta < 12^\circ$ and $w(\theta) = 0$ otherwise. For non-calibration particles which do

AMTD
5, 97–135, 2012

not meet the criteria for Mie-Lorenz theory other more complex scattering theories may be used to define the scattering intensity for Eq. (3). The impact upon misalignment of the optics of the CDP has been carried out by Lance et al. (2010) via raytracing but such analysis has not been performed upon the PCASP. It is estimated that the intersection point of the laser and sample can be displaced from the optics focal point by approximately 1 mm. This significantly impacts the 35° and 145° scattering angle limits and could cause them to vary by approximately 10°. It should be noted that for OPCs where particles are measured within the laser cavity of an external-cavity laser (so-called active cavity OPCs) Eq. (3) should be replaced with one of the sensitivity functions given by Pinnick et al. (2000).

Figure 1 shows scattering cross sections as a function of diameter for PSL spheres, DEHS and glass beads for the PCASP and CDP as well as other real world materials (assuming Mie-Lorenz theory) (Bond and Bergstrom, 2006; Dinar et al., 2006, 2008; Highwood et al., 2011; Muñoz et al., 2004; Patterson, 1981; Patterson et al., 1983; Toon, 1976; Wagner et al., 2011; Volten et al., 2001; Weast, 1966). It is clear that in general the curve is highly nonlinear and that above diameters of around 1 µm it is not monotonically increasing. Given the complexity of the Mie-Lorenz curve, the usual method of propagating uncertainty by multiplying by a function's gradient cannot in general be used. Instead we convert from diameter to cross section by integrating over a probability distribution function. Here we choose a normal distribution with standard deviation equal to the uncertainty in particle diameter. In this case the equivalent particle scattering cross section and its uncertainty for a particle diameter $\overline{D}_\mathrm{p} \pm \Delta D_\mathrm{p}$ is

$$\overline{\sigma}_\mathrm{p} = \frac{\int_0^\infty \sigma(D_\mathrm{p})\, G\left(D_\mathrm{p}\, \overline{D}_\mathrm{p},\, \Delta D_\mathrm{p}\right) d\, D_\mathrm{p}}{\int_0^\infty G\left(D_\mathrm{p}\, \overline{D}_\mathrm{p},\, \Delta D_\mathrm{p}\right) d\, D_\mathrm{p}} \tag{4}$$

and

AMTD
5, 97–135, 2012

$$\Delta\sigma_p = \sqrt{\frac{\int_0^\infty \left(\sigma_p(D_p) - \overline{\sigma}_p\right)^2 G\left(D_p\, \overline{D}_p,\, \Delta D_p\right) d\, D_p}{\int_0^\infty G\left(D_p\, \overline{D}_p,\, \Delta D_p\right) d\, D_p}} \quad (5)$$

where Δ represents uncertainty and $G(D_p, \overline{D}_p, \Delta D_p)$ is a Gaussian function of D_p with mean/mode $\overline{D}_p$ and standard deviation ΔD_p. Again because $\sigma_p(D_p)$ is a highly nonlinear function, $\overline{\sigma}_p$ will not in general be equal to $\sigma_p(\overline{D}_p)$. Converting the mode diameter of our calibration particles into cross section in this way ensures that the OPC is calibrated in terms of the property it directly measures. These calculations can be performed for any particles where scattering cross section is known as a function of diameter and are not dependent upon using Mie-Lorenz theory.

2.2 Calibration methods

2.2.1 Calibration introduction

Two different methods were used when calibrating the probes. A discrete method was used with the finite number of available PSL spheres and glass beads. A scanning method was also used with the DMA which allowed many closely spaced size distributions to be generated sequentially. Each of these methods is applicable to different calibration scenarios described in detail below

2.2.2 PCASP and CDP calibration setup

When calibrating the FAAM OPCs the instruments and sample generation equipment were set up as shown in Fig. 2. When calibrating the CDP a flow of air is forced through a vial of glass beads. These are suspended in the sample and directed through a guide to the sample area of the laser. Because the calibration particles are larger than a few micrometres, contamination from ambient air does not pose a problem. The flow rate

AMTD
5, 97–135, 2012

from the compressed gas supply is regulated in to provide a few hundred particles per second to the CDP. This is sufficiently low to minimise the effects of coincidence in the beam, yet high enough to provide a useful size distribution in a short time period. The concentration of smaller bead sizes in the sample tends to be more difficult to control which can result in high concentrations and coincidence of particles in the laser beam. Clumping of small particles, especially in moist conditions or when the air supply is cold, can also be a problem.

For the PCASP either nebulised PSL spheres or DEHS are used. When using DEHS a TSI model 3080 DMA with a 0.44 m column is used to provide a narrow size distribution. The sample is drawn through the DMA using the PCASP's pump. This requires the nosecone to be removed and the DMA output to be directly connected to the PCASP subsampler using a section of push on flexible tubing. When using nebulised PSL spheres the sample line may be directly connected to the subsampler as when using a DMA or the sample may be directed into the PCASP conical inlet in which case the positive pressure from the nebuliser pump floods the subsampler with the PSL loaded air. All tubing used is electrically conductive and as short as possible to minimise losses. Again a counting rate of a few hundred particles per second is used.

The nebuliser cup used in this work was an Allied Healthcare Aeromist model SA-BF61403. These cups can be operated using a pump or a compressed air supply using a needle valve to regulate flow.

2.2.3 Discrete method

Because an OPC measures scattering cross section directly it is possible to define a simple function which relates particle scattering cross section to pulse height. This function will be defined by the OPC detector and electronic systems. The PCASP and CDP use only linear amplifiers therefore we expect that pulse height will be a linear function of scattering cross section.

AMTD
5, 97–135, 2012

When calibrating an OPC in this manner there are two requirements.

1. The scattering cross sections of the calibration particles must be known.
2. The pulse heights measured by the OPC are known or, in cases where particles are binned into a histogram by the OPC, the bin boundaries must be known in terms of pulse height.

Simply knowing the manufacturer's estimate of bin boundary in terms of diameter is not sufficient unless the equivalent pulse height can be derived from these values.

For the PSL spheres and glass beads used in PCASP and CDP calibrations the scattering cross section along with an uncertainty were derived from Eqs. (3)–(5). This satisfies condition 1 above. The PCASP and CDP are both provided with a list of bin boundaries in terms of pulse height known as a threshold table. This table is modifiable to allow reprogramming of the instruments and satisfies condition 2 above making these OPCs suitable for use with this method.

To perform the calibration using PSL spheres and glass beads the PCASP and CDP are set up as shown in Fig. 2 and as described in Sect. 2.2.2. For calibrating the high gain stage of the PCASP only two useful sizes of PSL sphere were available to the authors' knowledge. Therefore another source of calibration particles was needed. In this case we made use of the DMA with nebulised DEHS aerosol. Using the DMA as set up in Fig. 2 values of D^* in the range 0.1–0.5 µm were set in steps of 0.003–0.01 µm. Using the DMA in this way ensured the generation of sufficient data points to effectively calibrate the high gain stage of the PCASP.

Both the PSL and DMA generated particle distributions have an uncertainty in their mean/mode diameter of just a few nanometres. Under normal use the PCASP has a resolution much wider than this which would dominate the uncertainty in the calibration. To reduce this uncertainty the PCASP is reprogrammed to zoom in on a particular size range of interest. In this way the uncertainties in particle diameter are comparable to the uncertainties in pulse height measured by the PCASP. For the CDP the setup is as in Fig. 2. It was not necessary to reprogram the CDP as its 30 bins over its single gain

AMTD
5, 97–135, 2012

stage contribute an uncertainty of similar magnitude to the calibration beads. Examples of the measured particle distributions as a function of pulse height are shown in Fig. 3 for PCASP and CDP.

To generate a calibration equation for the OPCs the mode particle scattering cross section is plotted against the mode pulse height measured by the OPC. The mode of the pulse heights is preferred to the mean because it is affected less by particle coincidence and contamination of the sample and can be used even when a part of the size distribution is outside the range of the OPC. In particular when using PSL spheres from solution, dried surfactant can generate significant contamination which can affect the distribution mean but not the mode.

Figure 4 shows example calibration data for the CDP and PCASP along with 1-σ uncertainties. Each data point represents a particular size of calibration particle. The uncertainties in scattering cross sections in Fig. 4 are derived from Eq. (5) and the uncertainties in pulse height are half the width of the modal bin in the measured particle distribution. The straight line fits to the data take into account uncertainties on both axes (Cameron Reed, 1989, 1992) to give a sensitivity, s, and offset V_0 along with uncertainties. We can then simply derive scattering cross section with uncertainty for any pulse height, V_{OPC}, as

$$\sigma_{\mathrm{OPC}} = V_0 + s\,V_{\mathrm{OPC}}, \tag{6}$$

$$\Delta\sigma^2_{\mathrm{OPC}} = \Delta V_0^2 + \Delta s^2\,V_i^2 + 2\,V_{\mathrm{OPC}}\,\mathrm{cov}(V_0 s), \tag{7}$$

where $\mathrm{cov}(V_0, s)$ is the covariance of the two variables.

The PCASP provides a single size distribution spanning all three gain stages. At the boundaries the gain stages overlap and in the overlap region particles are counted by only one gain stage. This causes a narrowing of one channel in each gain stage which should be trivial to account for from the calibration. Despite applying this information to the bin boundaries, artefacts in the size distribution always exist at these overlap points. These are discussed in more detail in Sect. 4.

AMTD
5, 97–135, 2012

2.2.4 Scanning method

For some OPCs it is not possible to easily record the pulse heights associated with each particle or with the bin boundaries. This may be because the pulse height measurements and binning are performed using analogue electronics which are not easy to characterise or it may be because the manufacturer does not make the information available to the user. In this case the OPC can be calibrated using a tuneable particle source where the particle size distribution may be adjusted in an almost continuous manner. This technique has been used to calibrate the FAAM PCASP using a DMA although the processing is more complex compared to the discrete method. Although this description is based upon using a DMA with a PCASP, any another OPC and particle source could be used, such as an impactor or a droplet generator in the supermicron range.

To calibrate the PCASP in this manner the equipment was set up as in Fig. 2 and particles in the range 0.1–0.5 µm in steps of 0.003–0.01 µm were passed through the DMA. As shown in Fig. 1, the scattering cross section monotonically increases with diameter in this range, hence, as the diameter of particles is increased the particle distribution moves to the higher bins on the PCASP. As the distribution crosses the bin boundary between bins n and $n+1$ we can examine the fraction of particles, F, in the bins above this boundary and use this parameter to determine its diameter equivalent. For an OPC with N bins measuring m_i particles in the ith bin and M particles in total we can define F as

$$F = \frac{\sum_{i=n+1}^{N} m_i}{M}. \quad (8)$$

For an OPC which does not bin particles into a histogram we can consider one bin to be the diameter/pulse height resolution of the instrument. The particle size distribution of the calibration aerosol, $P_p(D_p)$ can be related to F by

AMTD
5, 97–135, 2012

$$F = \frac{\int_{D_{bn}}^{\infty} P_p(D_p)\, d\, D_p}{\int_0^{\infty} P_p(D_p)\, d\, D_p} \quad (9)$$

where D_{bn} is the diameter of the boundary between bins n and $n+1$. It should be noted that Eq. (9) is based on the assumption that all of the particle size distribution falls within the range of the OPC and it is critical that this is verified during the calibration. As already discussed the particle scattering cross section for DEHS is monotonically increasing over the range where this technique is used, allowing us to use diameter in Eq. (9). For larger diameters D should be replaced by σ.

Because the DMA transfer function contains multiple peaks for multiply charged particles, as represented by n_e in Eq. (1), it is required that an OPC calibrated in this way has the resolution to identify the peaks representing $n_e > 1$ and that these peaks are discarded from the analysis. Alternatively these particles can be physically removed from the sample, for example by using an impactor.

When dealing with only a single peak it is possible to rigorously define $P(D_p)$ for Eq. (9) by applying the DMA transfer function from Eqs. (1) and (2) to the DEHS size distribution generated by the nebuliser (which can be assumed to be linear over a narrow size range). However, for the distributions used in this work it was found that F can be approximated by an integrated Gaussian (sigmoid) to within 1 % and doing so impacts the result by only ~0.1 %. Specifically

$$F \approx \frac{1}{2}\left(1 + \mathrm{erf}\left(\frac{D^* - D_{bn}}{\sqrt{2}\, W^2}\right)\right), \quad (10)$$

where the function erf is the error function and W is a measure of the distribution width. This function is much simpler than a more rigorous definition of F and also is likely to better represent random deviations from other uncertainties in the system. It is useful to note that due to the symmetry of Eq. (10) $F = 0.5$ when $D^* = D_{bn}$, i.e. when the mode of the DMA output is at a bin boundary 50 % of particles fall either side of the boundary.

AMTD
5, 97–135, 2012

To perform the calibration itself D^* is adjusted on the DMA scanning through the range of sizes over which the calibration is to be performed. For each value of D^* used a value of F is calculated using Eq. (8). Then for each bin, Eq. (10) is fitted to the data with D_{bn} and W as free parameters. The uncertainty in this estimate can be derived by combining the standard error output from the data fitting routine with the uncertainty in the DMA using the usual uncertainty combination functions.

A series of size distributions from a DMA calibration are shown in Fig. 5. The resolution is much poorer than in Fig. 3 because the bin boundaries for normal use are maintained for this calibration rather than zooming in on a region of interest. The secondary charged peak for the $D^* = 0.2\,\mu m$ spectrum is just visible, however it has been smeared out due to the resolution of the PCASP in this region of the size distribution. The number of particles counted in the doubly charged peak was more than 50 % of the number in the singly charged peak so it is clear this peak would have a large impact upon calculations of F if not discarded.

The values of F derived from all the size distributions collected as part of this calibration are shown in Fig. 6. The best fit curves are derived from Eq. (10). Each of the curves provides the upper boundary of one bin and in all cases the standard error in this boundary estimate is less than 0.3 % giving an uncertainty in bin width of between 1 and 10 %. In addition the uncertainty for the DMA is ~1 %. This is of a similar order to the discrete method.

3 Refractive index correction

As has already been stated the scattering cross section of a particle is a function of its refractive index n, diameter D_p, shape and structure. For OPCs calibrated using the discrete method above, applying this refractive index dependence is implicit in the conversion from scattering cross section to diameter. For an OPC calibrated in terms of diameter, such as when using a DMA to calibrate the submicron range of a PCASP as described above, then the bin boundaries must be first converted to scattering cross

AMTD
5, 97–135, 2012

section using Eqs. (3)–(5) for example. For a spherical particle Mie-Lorenz theory can be used perform the conversion from scattering cross section to diameter and although Fig. 1 shows that this is relatively straightforward for submicron particles it is clear that for supermicron particles where the Mie-Lorenz curves are not monotonic there are a number of challenges to overcome, for example:

- Multiple diameters may correspond to a single scattering cross section.
- The gradient at each solution will differ making uncertainties more difficult to interpret.
- The uncertainty may be large enough that the function significantly deviates from linear within a few error bars of the cross section of interest. This means that the uncertainty cannot be simply transformed using the function's gradient.

The first point above is highlighted particularly if we wish to derive the edges of an OPC bin in terms of diameter, then subtract one from the other to derive a bin width. It is very likely that the multiple solutions derived from the two boundaries will overlap in diameter space and the overlap may span most of the range of the solutions. Such a case is shown in Fig. 7 where the boundaries of a PCASP bin calibrated before the Fennec campaign are shown along with the Mie-Lorenz curve for PSL spheres.

Previously these problems have been worked around in a number of ways. Hand and Kreidenweis (2002) calibrated with aerosol of three different real refractive indices and used a polynomial interpolation for intermediate values. Lance et al. (2010) calibrated using particle of the same composition (water) as the particles measured in the real world. Others have smoothed theoretical curves or widened the bins of the OPC to generate a monotonically increasing function or reduce the effect of this ambiguity upon each bin (Johnson and Osborne, 2011; Liu et al., 1974). These methods either suffer from a lack of generality, being only applicable to particles of specified refractive indices or ranges of refractive indices, or requires a subjective assessment of the amount of smoothing required.

AMTD
5, 97–135, 2012

Here a rigorous method is presented which is general to any scattering function of arbitrary complexity without the need for smoothing. By examining Fig. 7 it is clear that in terms of diameter, each OPC bin has multiple boundaries. There are, however, other properties of a bin which provide enough information to derive a size distribution, can be described in terms of diameter, are easily visualised and may be rigorously defined. For normalisation purposes it is essential that we define the bin's width, W_b, which can be performed by summing the widths of all the sub-ranges highlighted by grey vertical bars in Fig. 7. By averaging the centres of the sub-ranges weighted by their widths we can also define a bin mean, $\overline{D}_b$, in terms of diameter. If there is a requirement to define the bins in terms of another quantity such as particle area, volume or log of diameter then the horizontal axis of Fig. 7 may be transformed appropriately. The bin mean and bin width defined in this way provide equivalent information to bin boundaries and so can be used as a direct replacement when calculating size distributions, mass/volume loadings and other derived quantities. The bin centre and bin width as described above are defined as

$$\overline{D}_{b_{perfect}}(\sigma_{bu}, \sigma_{bl}) = \frac{\int_0^\infty P(D, \sigma_{bu}, \sigma_{bl})\, D\, d\, D}{\int_0^\infty P(D, \sigma_{bu}, \sigma_{bl})\, d\, D} \tag{11}$$

$$W_{b_{perfect}}(\sigma_{bu}, \sigma_{bl}) = \int_0^\infty P(D, \sigma_{bu}, \sigma_{bl})\, d\, D \tag{12}$$

where $P(D, \sigma_{bu}, \sigma_{bl})$ is the probability that a particle with diameter D falls within a bin with upper and lower boundaries at σ_{bu} and σ_{bl}, i.e. $P(D, \sigma_{bu}, \sigma_{bl}) = 1$ when $\sigma_{bl} < \sigma(D) < \sigma_{bu}$ and 0 otherwise. The subscript perfect indicates that this is the perfect case with no uncertainties. It should be noted that values of $\overline{D}_b$ for adjacent bins may be closer or more distant than may be indicated by their widths. This is an effect of the interleaving of bins seen in Fig. 7 and a fundamental property of OPCs. Over a large diameter range any perceived overlaps or gaps will cancel.

AMTD
5, 97–135, 2012

If, as will always be the case in the real world, there are uncertainties associated with the bin boundaries then these must be propagated into our $\overline{D}_b$ and W_b. Two factors have a specific impact here. Because of the highly nonlinear Mie-Lorenz curve, the expectation for $\overline{D}_b$ and W_b may not be equal to $\overline{D}_{b_{perfect}}$ and $W_{b_{perfect}}$. Also the uncertainties in σ_{bl} and σ_{bu} will not be independent if they are derived from the same straight line fit, meaning that the usual uncertainty propagation formulae may not be usable.

If our best estimate of the bin's upper and lower boundary and their uncertainty are $\overline{\sigma}_{bl}$, $\overline{\sigma}_{bu}$, $\Delta\sigma_{bl}$ and $\Delta\sigma_{bu}$ then we can use these to generate a probability density function $w(\sigma_l, \sigma_u)$ that defines the probability that any estimate of σ_{bl} and σ_{bu} is the true boundary. If we calculate $\overline{D}_{b_{perfect}}$ and $W_{b_{perfect}}$ for a range of boundary estimates then we can integrate across the probability density function to define $\overline{D}_b$, W_b and their associated uncertainties as

$$\overline{D} = \frac{\int_0^\infty \int_0^\infty \overline{D}_{b_{perfect}}(\sigma_{bu}, \sigma_{bl})\, w(\sigma_{bu}, \sigma_{bl}) d\,\sigma_{bu}\, d\sigma_{bl}}{\int_0^\infty \int_0^\infty w(\sigma_{bu}, \sigma_{bl})\, d\sigma_{bu}\, d\sigma_{bl}}, \tag{13}$$

$$\Delta\overline{D}^2 = \frac{\int_0^\infty \int_0^\infty \left(\overline{D}_{b_{perfect}}(\sigma_{bu}, \sigma_{bl}) - \overline{D}\right)^2 w(\sigma_{bu}, \sigma_{bl})\, d\sigma_{bu}\, d\sigma_{bl}}{\int_0^\infty \int_0^\infty w(\sigma_{bu}, \sigma_{bl})\, d\sigma_{bu}\, d\sigma_{bl}}, \tag{14}$$

$$W = \frac{\int_0^\infty \int_0^\infty W_{b_{perfect}}(\sigma_{bu}, \sigma_{bl})\, w(\sigma_{bu}, \sigma_{bl})\, d\sigma_{bu}\, d\sigma_{bl}}{\int_0^\infty \int_0^\infty w(\sigma_{bu}, \sigma_{bl})\, d\sigma_{bu}\, d\sigma_{bl}}, \tag{15}$$

$$\Delta W^2 = \frac{\int_0^\infty \int_0^\infty \left(W_{b_{perfect}}(\sigma_{bu}, \sigma_{bl}) - W\right)^2 w(\sigma_{bu}, \sigma_{bl})\, d\sigma_{bu}\, d\sigma_{bl}}{\int_0^\infty \int_0^\infty w(\sigma_{bu}, \sigma_{bl})\, d\sigma_{bu}\, d\sigma_{bl}}. \tag{16}$$

AMTD
5, 97–135, 2012

Some careful consideration should go into the definition of $w(\sigma_{bl}, \sigma_{bu})$ as this function will not be the same in all cases. Where σ_{bl} and σ_{bu} are independent we can define $w(\sigma_{bl}, \sigma_{bu})$ as the product of two normal distributions.

$$w(\sigma_{bl}, \sigma_{bu}) = G\left(\sigma_{bl}, \overline{\sigma}_{bl}\, \Delta\sigma_{bl}\right) G\left(\sigma_{bu}, \overline{\sigma}_{bu}\, \Delta\sigma_{bu}\right). \quad (17)$$

This would be the case if the scanning calibration method has been used and the random uncertainties from the curve fitting dominate over any offset in particle diameter that may exist. This is not the case when σ_l and σ_u are derived from the same straight line fit. Instead $w(\sigma_{bl}, \sigma_{bu})$ can be defined with reference to the gradient and intercept of the straight line fit, their uncertainties and their covariance. Hence we replace w(σ_{bl}, σ_{bu}) with $w(s, V_0)$ and integrate over ds and dV_0 instead of σ_{bu} and σ_{bl} in Eqs. (15) to (17). The function $w(s, V_0)$ is defined by

$$w(s, V_0) = \frac{1}{2\,\pi\,\Delta s\,\Delta V_0} \exp\left(-\frac{\left[\frac{\left(s - \overline{s}\right)^2}{\Delta s} + \frac{\left(V_0 - \overline{V}_0\right)^2}{\Delta V_0} - \frac{2\,R\left(s - \overline{s}\right)\left(V_0 - \overline{V}_0\right)}{\Delta s\,\Delta V_0}\right]}{2\,\left(1 - R^2\right)} \right) \quad (18)$$

where R is the correlation coefficient between $\overline{s}$ and $\overline{V}_0$ defined as

$$R = \frac{cov\left(\overline{s}, \overline{V}_0\right)}{\Delta s\,\Delta V_0}. \quad (19)$$

The CDP is calibrated using the discrete method with a straight line fit so utilises Eq. (18). The PCASP's three separate gain stages are again calibrated using the discrete method so again Eq. (18) is used, however, at the point where the gain stages meet one bin has its lower boundary defined by one straight line fit and its upper boundary by another fit. This bin therefore has two independent boundaries so Eq. (17) is used here.

AMTD
5, 97–135, 2012

Although this method may seem complex it allows the refractive index correction to be determined directly from a Mie-Lorenz or another scattering curve, without the need for smoothing. In addition software tools have been developed and made freely available ensuring that performing these corrections becomes trivial.

4 Results and impact upon the Fennec dataset

In June 2011 the FAAM aircraft was deployed to the Sahara to make dynamics, radiation and dust measurements. The PCASP and CDP were employed to make measurements of particle concentrations and size distributions of desert dust and cloud particles and a part of this dataset is presented here. Prior to this campaign the PCASP and CDP were both calibrated using the discrete method described in Sect. 2 and the CDP was calibrated using the same method before each flight. Unfortunately a step change in the gain of the high gain stage of the PCASP is thought to have occurred between calibration and the beginning of the project and hence the first 6 bins of the PCASP have not been included here. It should also be noted that the first bins of the CDP and PCASP are routinely discarded as they do not have well defined lower boundaries.

As Fig. 7 shows, the actual ranges from a PCASP bin can vary significantly from the values provided by the manufacturer. In the calibration performed before Fennec the bin centres were found to be systematically higher than those reported by the manufacturer by an average of 13 % and a maximum of 33 ± 2 %. Monitoring the calibration results over approximately a year has shown that after routine maintenance, such as cleaning and aligning the optics, the calibration may change by up to 20 %. This result is consistent with the 35° and 145° limits of the PCASP collection optics varying by 10° as discussed in Sect. 2.1 The drift over time is typically much less than this and calibrations performed before and after projects which have lasted a month or more show less than 5 % drift.

AMTD
5, 97–135, 2012

During Fennec the CDP was calibrated before each flight apart from one and these have been examined to check the stability of the instrument over this time period. It was found that for all bins of the CDP the drift over the project was less than either the 2-σ uncertainty of the calibration or 9 %. The difference compared to the manufacture's nominal boundaries was found to be in the range 1.2 to 3.7 µm diameter. This equates to up to 15 % for bins 8 and above and up to 64 % for the smallest bin.

Size distributions from one time period during the Fennec project are shown here. This case consists of 150 s of data beginning at 10:10:30 UT and collected at 800 m above the surface (1080 m a.m.s.l. – above mean sea level). This was a measurement period with particularly high dust loadings. There is some uncertainty in the refractive index and shape of the dust measured and here it has been assumed that the dust particles are spheres with a refractive index of 1.53+0.003i which lies in the range measured by Wagner et al. (2011). Laboratory measurements have shown that Mie-Lorenz calculations can have some success in modelling the scattering properties of non-spherical particles. In the forward scattering angles, as measured by the CDP, laboratory measurements of bulk desert dust samples, including Saharan dust, agreed with Mie-Lorenz calculations within 20 % when surface area equivalent diameters were used (Volten et al., 2001; Kahnert et al., 2007). The scattering cross sections of ~0.2 µm salt particles as measured by a PCASP were modelled by Mie-Lorenz theory to within experimental uncertainties when mean crystal length equivalent diameter was used (Lui et al., 1992). It is beyond the scope of this paper to evaluate the many scattering theories which have been applied to nonspherical particles and hence based on the successes above Mie-Lorenz theory has been used.

The number and mass distributions as a function of particle diameter for the described time period are shown in Fig. 8. Distributions are compared using the manufacturer's specifications and calibrated, refractive index corrected bin boundaries. The distributions using the manufacturer's specification are discontinuous at the boundary between the two instruments around 4 µm and the PCASP data shows a zigzag in the distribution at 0.3 µm (the boundary between the mid and low gain stages) and a peak

AMTD
5, 97–135, 2012

in number concentration in the last channel. A similar zigzag is usually seen at the high to mid gain boundary at 0.14 µm. When a calibration is applied based upon the manufacturer's description of the instrument's function at the bin boundaries these features are not removed. Further investigation has indicated that some particles are not making the transition between gain stages despite being large enough to do so, resulting in an excess of particles in the top bin of a gain stage and a dearth in the first bin of the next gain stage. Merging the bins either side of a gain stage or reprogramming the PCASP so that one bin spans the gain stage boundary removes the zig-zag. This merging has been applied to the calibrated PCASP data in Fig. 8, in addition the final bin has been discarded.

The calibrated data can be seen to extend to much larger diameters than that processed using the manufacturer's specification. This is mostly due to the impact of the different refractive index of the measured dust and the PSL spheres and water droplets referenced by the manufacturer. The two instruments are in better agreement where they meet for the calibrated data, and the discontinuity seen in the size distributions based on the manufacturer's specification has been mostly removed. There is still a slight reduction in the concentrations measured in the first few bin of the CDP than needed to give an invisibly smooth transition between the two datasets, however, this reduction can be accounted for within the 2-σ uncertainties.

It is clear in the calibration case, however, that a dip in the distribution at diameters of ~1.3 µm has been enhanced rather than removed. This could be an instrument artefact caused by deviation of the probe geometry from the nominal collection angles or a difference between the real scattering properties and Mie-Lorenz theory predictions. There is a peak in scattering at ~35–40° predicted by Mi-Lorenz theory for particles of these diameters and this refractive index. This means the size distribution here is very sensitive to the exact location of the collecting optics' boundary or the details of the peak. A similar situation may occur for ~8 µm particles measured by the CDP.

It is of note that despite the distribution including particles of up to 100 µm diameter there is still a significant fraction of the mass missing from this distribution.

AMTD
5, 97–135, 2012

Measurements made by a shadow OPC during the project will enable the mass distribution to be continued to larger sizes and, due to its geometric measurement technique, will enable verification of the refractive index corrections.

5 Software tools

As part of developing the methods for the calibration and refractive index correction three software tools, known as MieConScat, PCASP Calibrator and CStoDConverter have been created. These are available to the community as open source projects free for academic use via the SourceForge repository (http://sourceforge.net). MieConScat generates particle scattering cross sections using Mie-Lorenz theory as described in Eq. (3). Text files can be saved giving particle cross section as a function of particle diameter, angular range, particle refractive index and wavelength of the incident light. This output can be used by the two subsequent programs.

PCASP Calibrator is a tool for analysing PCASP calibration data using the discrete method discussed in Sect. 2.2.3. Particle diameters are converted to cross sections, size distributions are generated, manual review and quality control can be performed and the modes of these distributions are used to generate a sensitivity curve for the three gain stages. This tool can use the output from MieConScat for deriving cross sections or text files can be generated by another method if Mie-Lorenz theory is not appropriate.

CStoDConverter accepts bin boundaries defined in terms of scattering cross sections and generates bin centres and widths in terms of diameter using the method described in Sect. 3. The conversion implicitly performs refractive index correction by using either the output from MieConScat or a similarly formatted text file generated any other way if Mie-Lorenz theory is not appropriate.

AMTD
5, 97–135, 2012

6 Conclusions

Two methods have been described here for calibrating Optical Particle Counters (OPCs) referred to as the discrete and scanning methods. The discrete method utilises particle samples available only at a finite number of different diameters and fits a sensitivity curve between the pulse height measured by the OPC and the scattering cross section of the particles. This method requires the user to have some access to the pulse heights measured by the OPC and has been used to calibrate a Passive Cavity Aerosol Spectrometer Probe (PCASP) and a Cloud Droplet Probe (CDP). The scanning method can be used when OPC pulse heights are not accessible but requires a sample size distribution which can be adjusted in a continuous manner. The PCASP has been calibrated using this method with a differential mobility analyser (DMA). The DMA provides a continuously adjustable sample of DEHS oil aerosol with mode diameter, D^*, up to 0.5 µm. A sigmoid-type function was fitted giving the fraction of particles larger than a given bin boundary, F, as a function of D^*. The diameter equivalent of the bin boundary is given by the value of D^* where F is equal to 0.5.

A transparent and mathematically well defined method for refractive index correction has been provided. This method allows OPC bin centres and widths to be defined using Mie-Lorenz theory or any other scattering theory. It can be applied even when particle scattering cross section as a function of diameter is highly nonlinear and not monotonic, thereby avoiding the need for smoothing. It also provides effective methods of uncertainty propagation.

Calibrating a PCASP and a CDP using these methods has shown that the PCASP differs up to 30 % and the CDP by up to 15–64 % from the manufacturer's specification and that a step change in calibration of up to 20 % can occur when routine maintenance is carried out. The drift in the calibration over a project with duration ∼1 month is better than 5 % for the PCASP and better than 9 % for the CDP. This calibration has shown inconsistencies with the expected behaviour where different gain stages of the PCASP meet. These can be overcome by discarding the upper bin of the PCASP and

AMTD
5, 97–135, 2012

reprogramming it to have a bin spanning each gain stage boundary or combining data from bins either side of gain stage boundaries. Desert dust size distributions collected by the PCASP and CDP as part of the Fennec project show a better agreement with each other and a general shift towards larger particle diameters (up to a factor of 3) when the calibration and refractive index corrections described here are applied. A dip in the PCASP size distribution at diameters of 1.3 µm and a less significant dip in the CDP at diameters of 8 µm may be caused by differences in the OPCs' geometry from nominal or a deviation of the dust particles from Mie-Lorenz theory.

In order that the community can implement similar calibration procedures and refractive index corrections with minimal effort a series of software tools with source code have been made available for community use. These are applicable not only to the PCASP and CDP but to other OPC models as well.

Some further work is required to continue to improve the data quality from the PCASP and CDP. The sampling efficiency of the PCASP should be derived for aircraft speeds, which may require a combination of inlet comparisons, wind tunnel tests and modelling. Methods for experimentally determining the optical geometry of both these instruments should be developed to attempt to reduce any artefacts in the measured size distributions.

Acknowledgements. The Fennec project was funded by the Natural Environment Research Council grant NE/G017166/1. We would like to acknowledge all the staff at Droplet Measurement Technologies who regularly work with the staff at FAAM to ensure that the instruments discussed here are in the best possible condition as well as Darrel Baumgardener for his useful comments regarding these instruments.

References

Belyaev, S. P. and Levin, L. M.: Techniques for collection of representative aerosol samples, J. Aerosol Sci., 5, 325–338, 1974.

Bond, T. C. and Bergstrom, R. W.: Light absorption by carbonaceous particles: an investigative review, Aerosol Sci. Tech. 40, 27–67, 2006.

AMTD

5, 97–135, 2012

Cai, Y., Montague, D. C., Wooiweer-Bryan, W., and Deshler, T.: Performance characteristics of the ultra high sensitivity aerosol spectrometer for particles between 55 and 800 nm: Laboratory and field studies, J. Aerosol Sci., 39, 759–769, 2008.

Cameron Reed, B.: Linear least-squares fits with errors in both coordinates, Am. J. Phys., 57, 642–646, 1989.

Cameron Reed, B.: Linear least-squares fits with errors in both coordinates, II: Comments on parameter variances, Am. J. Phys., 60, 59–62, 1992.

Cook, J., Highwood, E. J., Coe, H., Formenti, P., Haywood, J. M., and Crosier, J.: A comparison of aerosol optical and chemical properties over the Adriatic and Black Seas during summer 2004: Two case-studies from ADRIEX, Q. J. Roy. Meteorol. Soc., 133, 33–45, 2007.

Cotton, R., Osborne, S., Ulanowski, Z., Kaye, P. H., and Greenaway, R. S.: The ability of the mall Ice Detector (SID-2) to characterize cloud particle and aerosol morphologies obtained during flights of the FAAM BAe-146 Research Aircraft, J. Atmos. Ocean Tech., 27, 290–303, 2010.

Dick, W. D., Ziemann, P. J., Huang, P., and McMurry, P. H.: Optical shape fraction measurements of submicrometre laboratory and atmospheric aerosols, Meas. Sci. Technol., 9, 183–196, 1998.

Dinar, E., Mentel, T. F., and Rudich, Y.: The density of humic acids and humic like substances (HULIS) from fresh and aged wood burning and pollution aerosol particles, Atmos. Chem. Phys., 6, 5213–5224, doi:10.5194/acp-6-5213-2006, 2006.

Dubovik, O., Sinyuk, A., Lapyonok, T., Holben, B. N., Mishchenko, M., Yang, P., Eck, T. F., Volten, H., Muñoz, O., Veihelmann, B., van der Zande, W., Leon, J., Sorokin, M., and Slutsker, I.: Application of spheroid models to account for aerosol particle nonsphericity in remote sensing of desert dust, J. Geophys. Res., 111, D11208, doi:10.1029/2005JD006619, 2006.

Hand, J. L. and Kreidenweis, S. M.: A New Method for Retrieving Particle Refractive Index and Effective Density from Aerosol Size Distribution Data, Aerosol Sci. Tech., 36, 1012–1026, 2002.

Highwood, E. J., Northway, M. J., McMeeking, G. R., Morgan, W. T., Liu, D., Osborne, S., Bower, K., Coe, H., Ryder, C., and Williams, P.: Scattering and absorption by aerosols during EUCAARI-LONGREX: can airborne measurements and models agree?, Atmos. Chem. Phys. Discuss., 11, 18487–18525, doi:10.5194/acpd-11-18487-2011, 2011.

AMTD
5, 97–135, 2012

Hudson, P. K., Gibson, E. R., Young, M. A., Kleiber, P. D., and Grassian, V. H.: A Newly Designed and Constructed Instrument for Coupled Infrared Extinction and Size Distribution Measurements of Aerosols, Aerosol Sci. Tech., 41, 701–710, 2007.

Johnson, B. T. and Osborne, S. R.: Physical and optical properties of mineral dust aerosol measured by aircraft during the GERBILS campaign, Q. J. Roy. Meteorol. Soc., 137, 1117–1130, 2011.

Knutson, E. O. and Whiteby, K. T,: Aerosol classification by electric mobility: apparatus, theory, and applications, J. Aerosol Sci., 6, 443–451, 1975.

Lance, S., Brock, C. A., Rogers, D., and Gordon, J. A.: Water droplet calibration of the Cloud Droplet Probe (CDP) and in-flight performance in liquid, ice and mixed-phase clouds during ARCPAC, Atmos. Meas. Tech., 3, 1683–1706, doi:10.5194/amt-3-1683-2010, 2010.

Liu, B. Y. H., Berglund, R. N., and Agarwal, H. K.: Experimental studies of Optical Particle Counters, Atmos. Environ., 8, 717–732, 1974.

Liu, P. S. K., Leaitch, W. R., Strapp, J. W., and Wasey, M. A.: Response of Particle Measuring Systems Airborne ASASP and PCASP to NaCl and Latex Particles, Aerosol Sci. Tech., 16, 83–95, 1992.

Muñoz, O., Volten, H., Hovenier, J. W., Veihelmann, B., van der Zande, W. J., Waters, L. B. F. M., and Rose, W. I.: Scattering matrices of volcanic ash particles of Mount, St. Helens, Redoubt, and Mount Spurr Volcanoes, J. Geophys. Res., 109, D116201, doi:10.1029/2004JD004684, 2004.

Patterson, E. M.: Measurements of the imaginary part of the refractive index between 300 and 700 nanometers for Mount St. Helens Ash, Science, 211, 836–838, 1981.

Patterson, E. M., Pollard, C. O., and Galindo, I.: Optical Properties of the ash from El Chichon volcano, Geophys. Res. Lett., 10, 317–320, 1983.

Pinnick, R. G., Pendleton, J. D., and Videen, G.: Response Characteristics of the Particle Measuring Systems Active Scattering Aerosol Spectrometer Probes, Aerosol Sci. Tech., 33, 334–352, 2000.

Tegan, I. and Fung, I.: Contribution to the aerosol mineral load from land surface modifications, J. Geophys. Res., 100, 18707–18726, 1995.

Toon, O. B., Pollack, J. B., and Khare, B. N.: The optical constants of several atmospheric aerosol species: ammonium sulphate, aluminium oxide and sodium chloride, J. Geophys. Res., 81, 5733–5748, 1996.

AMTD
5, 97–135, 2012

Volten, H., Muñoz, O., Rol, E., de Haan, J. F., Vassen, W., Hovenier, J. W., Muinonen, K., and Nousiainen, T.: Scattering matrices of mineral aerosol particles at 441.6 nm and 632.8 nm, J. Geophys. Res., 106, 17375–17401, 2001.

Wagner, R., Ajtai, T., Kandler, K., Lieke, K., Linke, C., Müller, T., Schnaiter, M., and Vragel, M.: Complex refractive indices of Saharan dust samples at visible and near UV wavelengths: a laboratory study, Atmos. Chem. Phys. Discuss., 11, 21363–21427, doi:10.5194/acpd-11-21363-2011, 2011.

Wiscombe, W. J.: Improved Mie scattering algorithms, Appl. Optics, 19, 1505–1509, 1980.

AMTD

5, 97–135, 2012

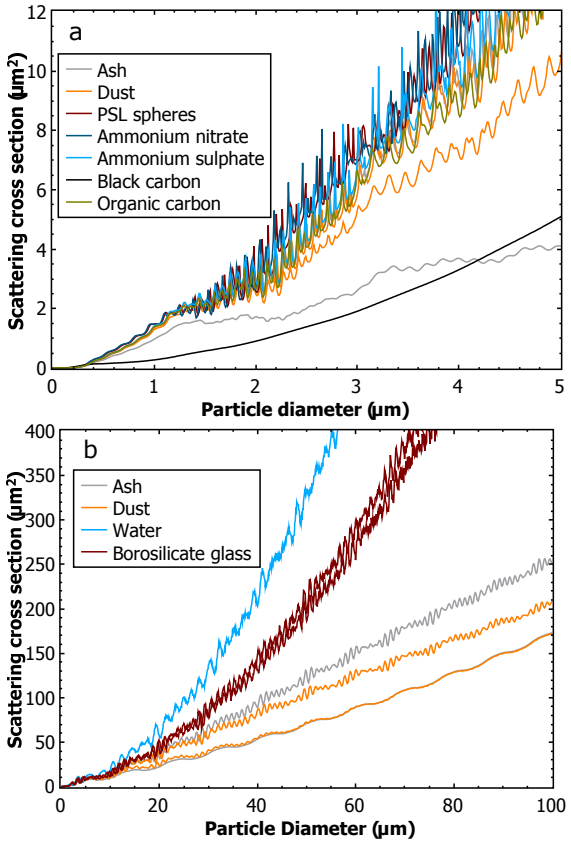

Fig. 1. Mie-Lorenz curves showing scattering cross sections for a variety of materials as measured by a PCASP **(a)** and a CDP **(b)**. The two curves for Saharan dust and volcanic ash approximately bound a range of refractive indices found in the literature. For borosilicate glass the two curves represent the two different refractive indices given by the manufacturer for different samples of calibration beads.

AMTD
5, 97–135, 2012

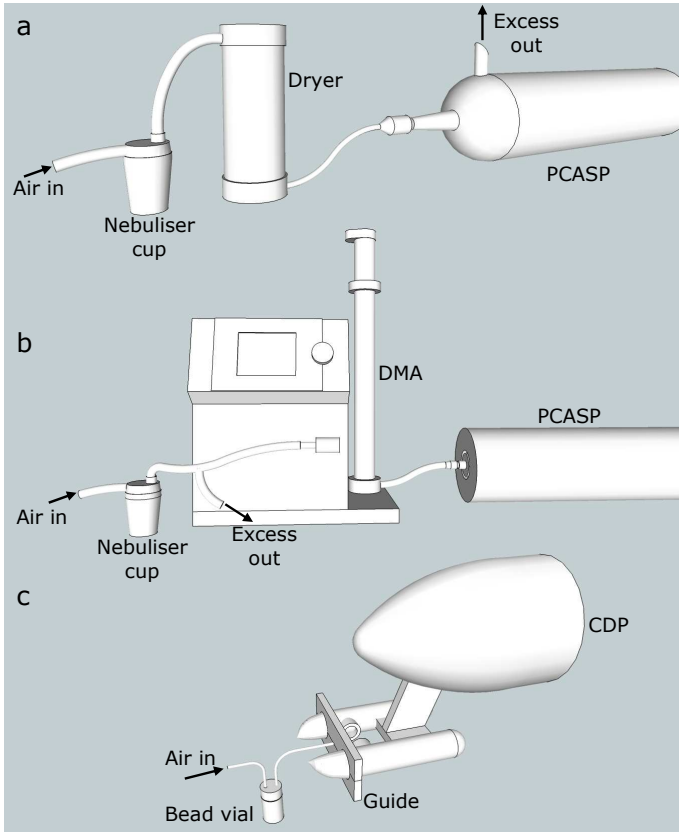

Fig. 2. Calibration setup for the PCASP and CDP OPCs. The PCASP is either calibrated using nebulised PSL spheres **(a)** or a DMA with nebulised DEHS oil aerosol **(b)** and the CDP is calibrated with dry dispersed glass beads **(c)**. When used with the DMA the PCASP conical inlet is removed and the sample line is connected directly to the subsampler. During calibration of the CDP a guide attaches to the instrument arms to direct the sample into the sensitive volume.

AMTD
5, 97–135, 2012

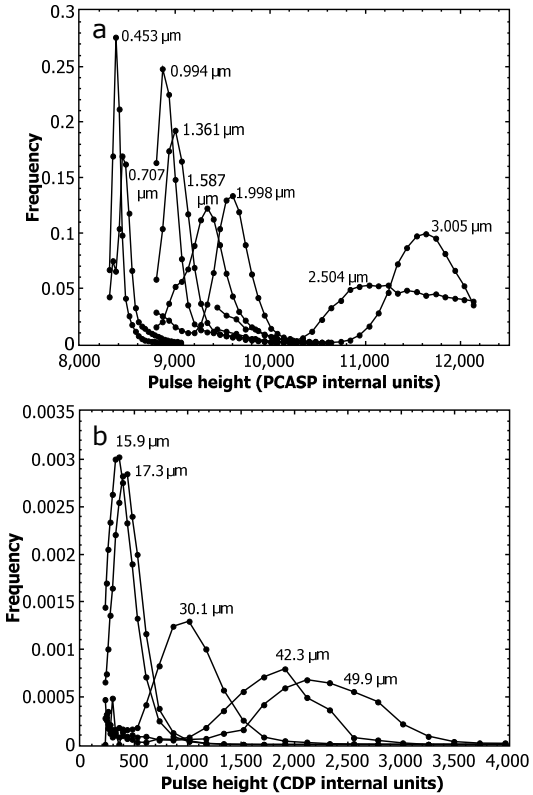

Fig. 3. Particle size distributions generated during calibration of the PCASP **(a)** and CDP **(b)** with labels indicating the mode diameter of the distribution. The distributions have been normalised to give an area under each curve of unity. For the PCASP only a subset of the used PSL sphere size distributions are shown and the high resolution is achieved by reprogramming the instrument to zoom in on the area of interest. The broad distribution for the 2.504 µm spheres may be cause by the close proximity to a spike in the Mie-Lorenze curve. The CDP calibration size distributions were generated using glass beads.

AMTD
5, 97–135, 2012

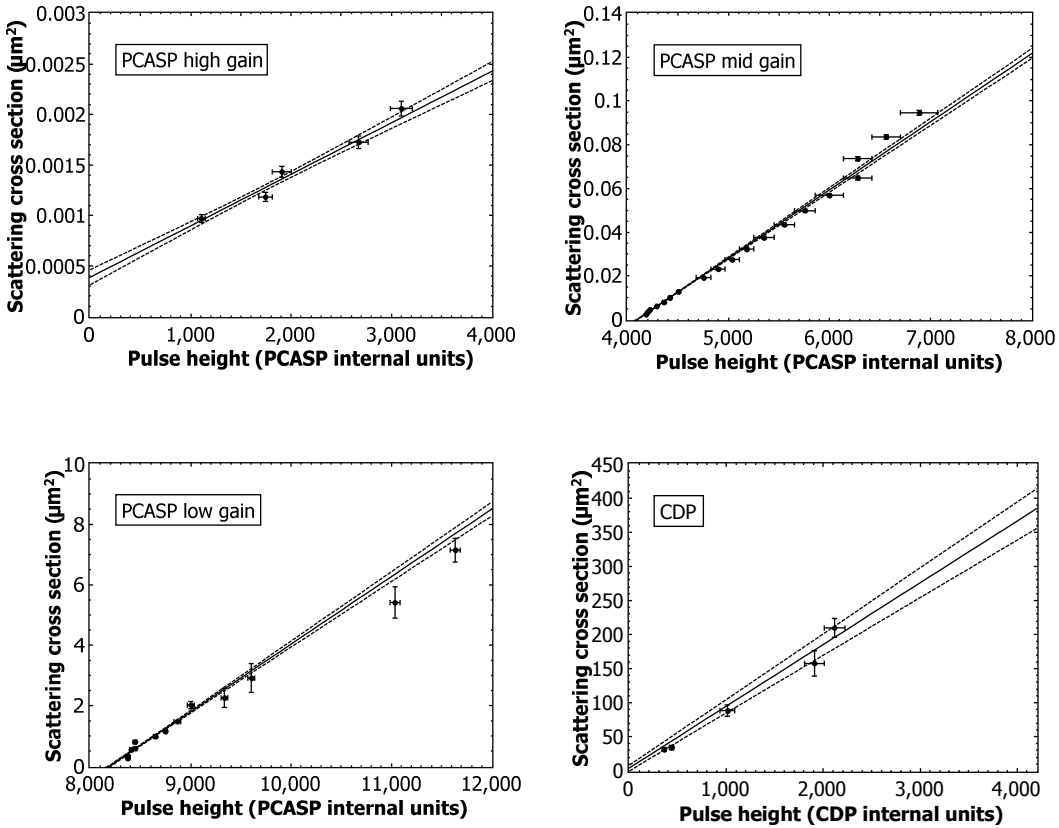

Fig. 4. Particle scattering cross section as a function of pulse height for an example calibration of the PCASP and CDP. The points represent the modes of size distributions generated from calibration particles with scattering cross sections defined by Eq. (4). The uncertainties in the x direction are defined as half the OPC resolution and those in the y direction are defined by Eq. (5). The solid line shows the best fit straight line when uncertainties on both axes are utilised dashed line shows the standard error of the best fit.

AMTD
5, 97–135, 2012

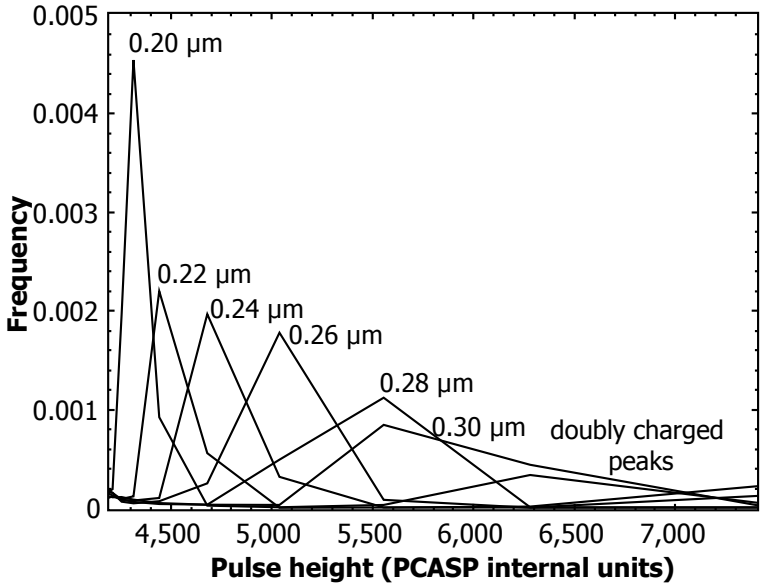

Fig. 5. Particle size distributions measured during a scanning calibration of a PCASP using a DMA. Each bin is normalised by dividing by its width and each size distribution is then normalised to give a total area under each curve of 1. The resolution here is not as good as in Fig. 3 as the bin boundaries used here are those for normal use and no zooming in is applied. Only the mid gain stage is shown. For pulse heights above approximately 6000 peaks can be seen from particles with double charges which pass through the DMA. The peak at 6300 is the doubly charged peak from $D^* = 0.20$ and contains more than one third of the total particles in this distribution. These extra peaks must be removed from the analysis to avoid biasing the calibration results.

AMTD
5, 97–135, 2012

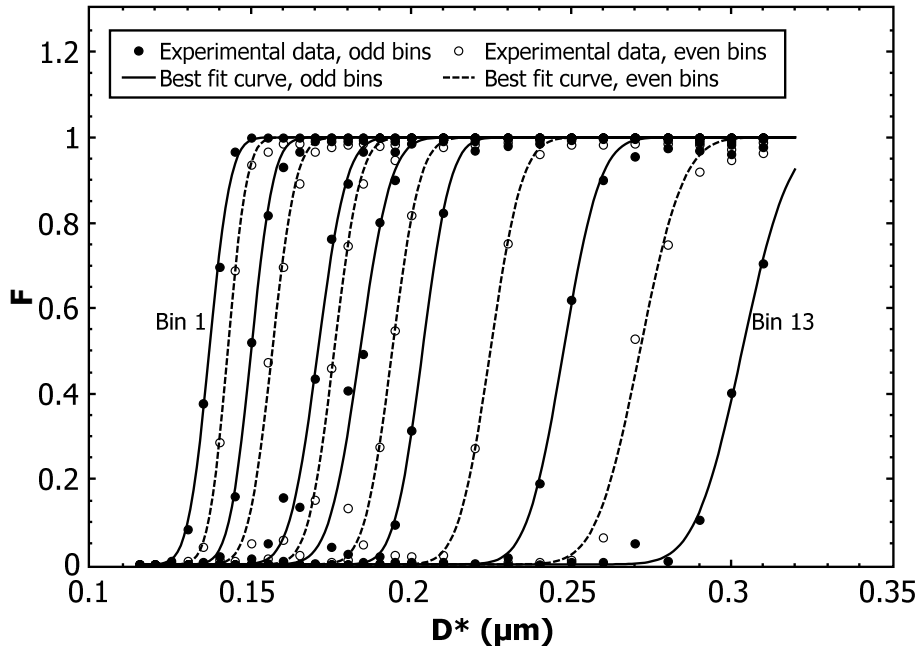

Fig. 6. An example scanning calibration result using a DMA with a PCASP. Each curve represents one bin boundary and shows how the fraction of particles bigger than this boundary, F, increases as the DMA mode diameter, D^*, increases. The value of D^* at which a best fit curves cross 0.5 defines the boundary's equivalent diameter. Multiply charged particles from the DMA were screened out during the data analysis.

AMTD
5, 97–135, 2012

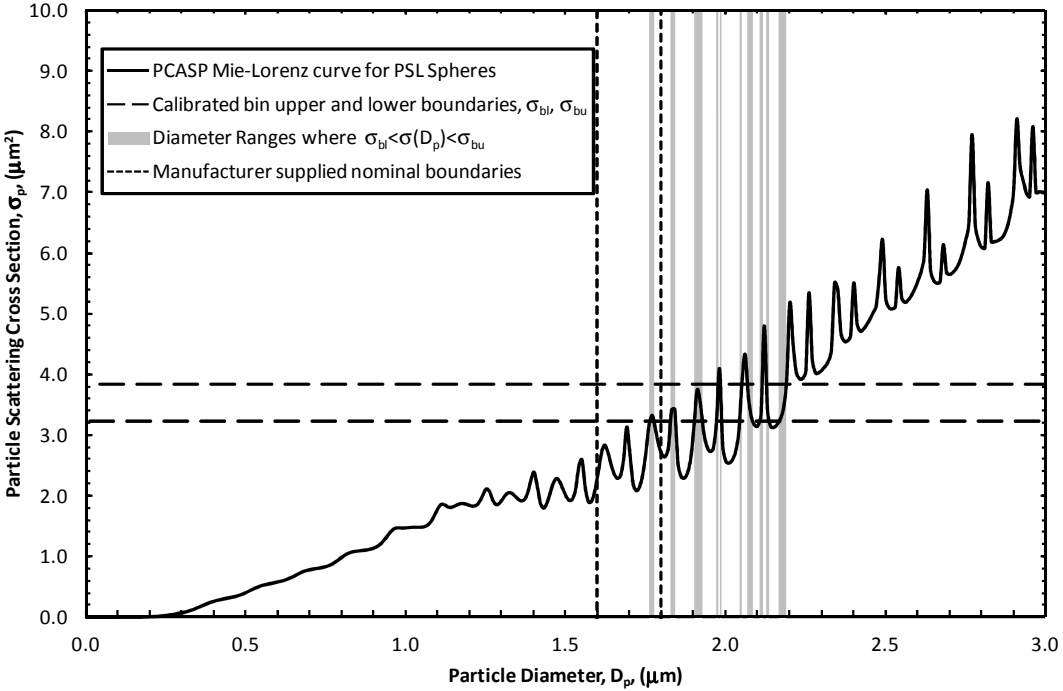

Fig. 7. Example showing the range of sizes of PSL spheres which would fall within a single bin of a PCASP. The grey shading covers all diameter ranges where the Mie-Lorenz curve falls between the horizontal dashed lines derived from calibration. The vertical dotted lines show the manufacturer's boundaries for the same bin.

AMTD
5, 97–135, 2012

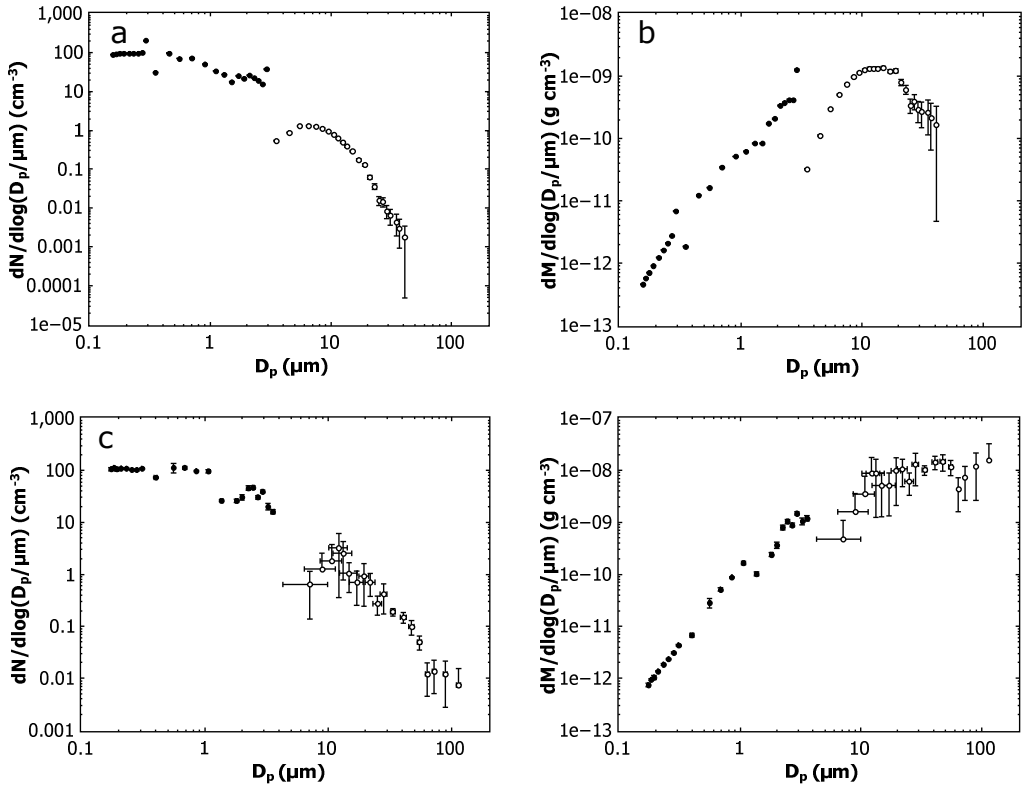

Fig. 8. Size distribution of desert dust aerosol measured by the PCASP (filled circles) and CDP (open circles) during a run at 800 m above the surface. Plots show the distributions derived using the manufacturer's specification based on the refractive index of PSL spheres **(a, b)** and the distributions derived from calibrated refractive index corrected data **(c, d)**. The number, N, and mass, M, are shown as a function of particle diameter D_p. The density of dust has been assumed to be 2.65 g cm^{-3} (Tegan and Fung, 1995) and error bars which extend to negative numbers on the log scale have been omitted for clarity.

AMTD
5, 97–135, 2012